Direct experimental evidence of growing dynamic length scales in confined colloidal liquids

Prasad S. Sarangapani, Andrew B. Schofield, and Yingxi Zhu

Phys. Rev. E **83**, 030502 — Published 28 March 2011

DOI: 10.1103/PhysRevE.83.030502

Direct Experimental Evidence of Growing Dynamic Length Scales in Confined Colloidal Liquids

Prasad S. Sarangapani[1], Andrew B. Schofield[2], and Yingxi Zhu[1,*]

[1] Dept. of Chemical and Biomolecular Engineering

Univ. of Notre Dame, Notre Dame, IN 46556, USA

[2] School of Physics, Univ. of Edinburgh, Kings Buildings

Edinburgh EH9 3JZ, UK

Abstract

The modification of the glass transition in confined domains, particularly the length scales associated with cooperative motion, remains a mystery. Hard-sphere suspensions are confined between two surfaces to progressively smaller dimensions to probe the confinement effect on the growth of dynamic heterogeneities via confocal microscopy. The confinement length scale is defined as the critical spacing where deviations from bulk behaviors begin and is observed to occur at progressively larger gaps as the volume fraction is increased. However, dynamic length scales extracted from the four-point correlation function are on average smaller than the confinement length scale.

* Author to whom correspondence should be addressed (Email: yzhu3@nd.edu).

PACS numbers: 64.70.pv, 68.15.+e, 83.10.Tv

Soft matter confined between surfaces or at interfaces occurs ubiquitously in nature and modern technological applications [1-3]. Despite extensive interest and activity of research in this area, major questions regarding the modification of material properties in confined domains remain. Among the myriad physical phenomena observed in confined domains, the modification of the glass transition temperature, T_g, in confinement has received the most attention yet remains contentious [4, 5]. Understanding the nature of the glass transition in confinement has significant impact on many unresolved problems ranging from the instability of sub-100 nm polymer nanostructures in data storage applications to protein folding [6, 7].

Interest in the confinement effect on the *dynamics* close to the glass transition was initially motivated by the desire to extract a "dynamic" length scale of molecular cooperativity, which is often masked in ensemble-averaged measures [8]. When a super-cooled liquid is confined to a critical dimension where strong deviations from bulk behaviors occur, a dynamic length scale for the glass transition can be possibly obtained [9]. However, in search of this parameter, numerous experiments [4, 8-16] and computer simulations [4-6] with freestanding polymer thin films as well as glass formers confined in nanopores have produced contradictory results: T_g can increase [8], decrease [4, 10], or remain the same [16], depending on the nature of molecule-surface interactions.

The length scales for the onset of the confinement effect on glass forming liquids, commonly referred to as the "confinement length scale", have also been reported in the literature [10]. Computer simulations have predicted that the confinement length scale is typically larger than the size of cooperatively rearranging regions [17], which implies that the confinement length scales are *not* representative of the length scales associated with dynamical heterogeneities. Both confinement and dynamic length scales have been extracted from

experimental data [18], however the correlation between these two length scales has not been explored experimentally.

Colloidal hard-spheres have been proven as excellent model systems to study the glass transition with the distinct advantage of facile and direct visualization using a surfeit of microscopic methods ranging from wide-field microscopy to confocal scanning microscopy [19, 20]. Using confocal microscopy, direct access to dynamical heterogeneities in dense "super-cooled" colloidal liquids in three-dimensions becomes possible and this technique has been used to further understanding of the dynamics of bulk, glassy systems and confirmed key theories [21] and predictions from computer simulations [22] relating to the glass transition. In this study, we extend our previous work, which has demonstrated a significant slowing down of the dynamics of hard-sphere colloidal suspensions in confinement [23], to probe the relationship between the growth of dynamical heterogeneities and the confinement length scale – a subject that remains experimentally unexplored hitherto. Our findings reported in this Letter show, *for the first time from direct experimental evidence*, that the growing length scales of dynamical heterogeneities are, on average, smaller than the confinement length scale, despite both strongly depending on volume fraction.

Our model hard-sphere system consists of poly(methyl methacrylate) (PMMA) suspensions (diameter, d=1.288 μm, polydispersity <5%), sterically stabilized and impregnated with rhodamine 6G for direct visualization via confocal microscopy [24]. The particles are suspended in dioctyl phthalate which matches the index of refraction of the particles (n = 1.494). Sedimentation is not observed for undisturbed samples over a period >>1 year. Volume fractions ranging from ϕ = 0.40-0.57 with an uncertainty of ±0.03 are prepared and subsequently verified using Voronoi tessellation [20]. We observe no deviations from the bulk volume fraction for the

range of film thicknesses probed in our experiments [25]. A home built micron-gap compression apparatus as previously described [23] is mounted on the stage of a confocal microscope (Zeiss LSM 5 Pascal, 100x objective, NA = 1.4) where thicknesses, H are explored over a range of H/d from ≈78 down to ≈11. Boundary induced crystallization, which would be otherwise induced between smooth walls, is prevented by coating ~1-2 disordered layers of sterically stabilized PMMA particles (polydispersity ~ 18%) [26] on each confining quartz surface and subsequently sintered at T = 110 ^{o}C for 40 minutes. A 10 x 10 mm^2 sample well is attached to the confining surfaces using UV-curing optical adhesive (Norland 80) and injected with ~200 μL of PMMA suspensions. A waiting period of at least five hours is required for density profiles to homogenize before experiments commence, which is a necessary step to minimize any change in the overall volume fraction during compression, otherwise leading to the formation of "depletion layers" [23]. We systematically reduce the gap spacing between two solid surfaces using a high precision micrometer (Newport) at a rate of 2 μm/min with an interval of 10-15 minutes between two successive compression steps to allow the dissipation of any transient flow. At each desired film thickness, we wait a minimum of four hours before image acquisition. Film thickness is determined solely from z-stacks with an accuracy of ±0.2 μm. A 30 x 30 x 12 μm^3 volume containing ~3000 particles is scanned every 14 seconds for ~16 hours. Three-dimensional particle centroiding algorithms [27] are subsequently employed to determine particle centers with an accuracy of 0.05 μm in the x-y plane and 0.2 μm in the z-direction.

We start by examining the nature of single particle displacements in confined colloidal liquids. In both bulk and confined domains, the dynamics of liquids close to the glass transition become increasingly intermittent and the rearrangements of particles are cooperative. Previous work on bulk molecular and colloidal liquids in proximity to the glass transition has shown that

the distribution of particle displacements deviates from a Gaussian on the timescales of cage rearrangements, which is related to the late β relaxation regime [20, 21]. Deviations from a Gaussian are quantified in terms of the non-Gaussian parameter, α_2, which, for a one-dimensional distribution of displacements, is defined as $\alpha_2 = \langle x^4 \rangle / 3\left(\langle x^2 \rangle\right)^2 - 1$ (Eq.1). This measure is most sensitive to a sub-ensemble of particles contributing to irreversible rearrangements in liquids [20]. For a Gaussian distribution of particle displacements, $\alpha_2 \approx 0$, while $\alpha_2 > 0$ for the case where a significant fraction of particles undergo larger-than-average displacements. We have examined α_2 in the x, y, and z directions for confined PMMA colloidal suspensions; however, we only show the results for particle motions parallel to the walls in Figure 1, owing to poor resolution in the z-direction that is inherent in confocal microscopy of dense colloidal systems. It is evident that the dynamics become more heterogeneous as thickness is reduced. At any time only a small number of rare "mobile" particles contribute to the growth of the non-Gaussian parameter. It is conceivable that as the film thickness is reduced, more mobile particles contribute to the tails of the probability distribution of displacements.

To further explore whether the dynamics of mobile particles is indeed facilitated, we examine the angles formed between the displacement vectors of all neighboring particles defined as $\theta = \cos^{-1}(\Delta\vec{r}_i \cdot \Delta\vec{r}_j / |\Delta\vec{r}_i||\Delta\vec{r}_j|)$ at timescales corresponding to the peak in α_2 at varied H/d and ϕ. In Fig. 2a-c we plot $P(\theta)$ for $\phi = 0.40 - 0.46$. As H/d is decreased, the propensity for coherent motion of particles is greater, where at the narrowest gap, H/d=11, $P(\theta)$ is strongly peaked at $\theta \approx 0$, indicating large groups of particles move in a similar direction, as schematically illustrated in Fig. 2d-e for $\phi = 0.40$ and 0.43 at H/d=11, respectively. It is apparent that confinement enhances the tendency of particles to move in parallel directions; such a behavior likely originates from the slow dynamics of particles immediately adjacent to the surfaces [12, 28] , as they are essentially

caged and the slow dynamics subsequently propagate to the interior of confined colloidal film. The influence of the walls clearly becomes much stronger at narrow gaps, thereby resulting in particles exhibiting cooperative "string-like" dynamics. This picture is qualitatively consistent with the simulation results of super-cooled liquids confined in pores of controlled roughness, where the slow dynamics induced by *rough* walls may propagates to adjacent layers of the confined liquid [12] and increases the tendency of facilitated motion at narrow gaps, resulting in the enhancement of dynamic heterogeneity.

While α_2 and $P(\theta)$ show the strong evidence of dynamical heterogeneity, these measures do not provide a way to measure the growing *dynamic length scales* in confinement. To find the length scales of dynamic heterogeneity associated with confined colloidal thin films, it is necessary to determine the correlations in the dynamics at two different points in time and space by using the four-point correlation function, $g_4(r,\tau)$ [29] defined as: $g_4(r,\tau) = \frac{1}{N\rho}\langle\sum_{ijkl}\delta[r + r_i(0) + r_k(0)]\, w(r_i(0) - r_j(\tau)) \times w(r_k(0) - r_l(\tau))\rangle - \langle\frac{Q(\tau)}{N}\rangle^2$ $(Eq.2)$, where the first term is a pair-correlation function for overlapping particles, $g_4^{ol}(r, \tau)$ and the second term is the squared mean overlaps, defined as $Q(\tau)=w(r_i(0) - r_j(\tau))$ where w is an overlapping function which is unity if $w\left(\left|r_i(0) - r_j(\tau)\right|\right), w\left(\left|r_k(0) - r_l(\tau)\right|\right) \le a$ and zero otherwise, where "a" (≈0.63 μm) is chosen to be the radius of our PMMA particles. We find that our choice of "a" provides the best distinction between localized and delocalized particles in our system and ensures the reproducibility of $g_4(r, \tau)$ obtained from independent data sets. In this study, we examine $g_4^{*}(r,\tau) = g_4^{ol}(r,\tau)/\langle Q(\tau)/N\rangle^2 - 1$. We show $g_4^{*}(r, \tau)$ at varied lag times and film thickness for a suspension with ϕ = 0.40 and 0.43 in Fig. 3a-f, it is clear that the four-point correlation function captures the dynamic heterogeneity where the range of dynamical correlations are maximal at

some intermediate time and also decrease on longer time scales, which is consistent with prior studies of this measure [29].

We choose to use an "envelope fitting" method to extract dynamic length scales, ξ_4, directly from $g_4^*(r, \tau)$ on timescales where ξ_4 is maximal [30], using the relation $g_4^*(r,\tau) = A\exp(-r/\xi_4)$ over a range of 2 μm < r < 9 μm, where A is a freely floating constant. This fitting procedure has been demonstrated to be successful in simulated super-cooled liquids [29, 31]. As shown in Figure 3g, it is clear that ξ_4 for $\phi = 0.40$ and 0.43 grows precipitously as H/d is reduced. However, as ϕ increases toward $\phi = 0.58$ for the bulk colloidal glass transition, the effect of confinement on dynamic length scales appears much weaker. It should be noted that upon examining all the data across varied ϕ, there is indeed an apparent drop in dynamical heterogeneities when the bulk colloidal glass transition at $\phi = 0.58$ is approached, reflecting the competition between increasingly constrained dynamics at high volume fractions and dynamical fluctuations to relax the system over large length scales [31].

The four-point correlation function reveals the length scales associated with *dynamical heterogeneities.* However, it is also of great interest to examine the ϕ-dependence on the critical dimension where spatial confinement has an effect on dynamics, thereby yielding an *additional length scale for the glass transition,* designated as the confinement length scale, ξ_{conf}. To extract ξ_{conf}, we examine the H/d-dependence on mean square displacements (see Supplementary Fig.2), four-point susceptibility (see Supplementary Fig. 3), and α_2 for varied ϕ and pool the results to examine if there is a critical confinement length scale common to all of our measures as well as independent data sets. We define the confinement length scale as the critical thickness where deviations from bulk behavior begin to occur in all the measures examined in this study, represented as a dash line in Fig. 1 as well as Supplementary Fig. 2 and 3. Indeed, we do find the

ϕ-dependent ξ_{conf} as shown in Figure 4. Simulations [1] have found that the length scales for dynamical heterogeneities are significantly smaller than the confinement length scale [19], which is also found to be the case for all the samples we have investigated in this work. Our results indicate that confinement results in a decrease in ϕ_g, which is analogous to an increase in T_g in the case of molecular liquids. To check our conjecture we rescale the four-point susceptibilities and investigate whether there is indeed a density-thickness super-position principle. Indeed, upon rescaling the four-point susceptibilities of confined PMMA of variedϕ with respect to a bulk suspension of $\phi = 0.40$, we find that all the data at varied ϕ can be collapsed into a single master curve (see Supplemental Figure 4); as a result, a plot of the shift factors against relative thickness is obtained to clearly indicate that ϕ_g *decreases in confinement*.

In summary, we have demonstrated that confinement has a strong influence on dynamics: Confined colloidal hard-spheres show a significant reduction in ϕ_g, which is accompanied by a marked increase in cooperative dynamics in confinement as the gap spacing becomes smaller than the confinement length scale. However, the effect of confinement on dynamics becomes weaker for higher ϕ as evidenced by the film thickness dependence on the dynamic length scales for $\phi = 0.46$ and 0.57 where an apparent drop in dynamic heterogeneity is observed at $\phi = 0.57$. Significantly, dynamic length scales extracted from the four-point correlation functions are on average smaller than the confinement length scale, despite both strongly depending on volume fraction. It could be interesting to further explore the relationship between structure and dynamics for binary colloidal suspensions under confinement. The shapes of rearranging regions observed in ref [33] for binary hard-sphere suspensions may be a consequence of changes in local structure as well.

Acknowledgement. PSS and YZ are grateful for financial support from the National Science Foundation under grant No. CBET-0730813 and CMMI-100429.

References

1. S. Granick, Physics Today **52,** 26 (1999).
2. Y. Ding, H.W. Ro, T.A. Germer et al, ACS Nano **1**, 84 (2007).
3. G.Y. Jung, S. Ganapathiappan, D.A. Ohlberg et al, Nano Lett. **4**, 1225 (2004).
4. C.L. Jackson and G.B. McKenna, J. Non-Cryst. Solids **131**, 221 (1991).
5. M. Alcoutalbi and G.B. McKenna, J. Phys: Cond. Matt. **17**, R461 (2005).
6. K.V. Workum and J.J. de Pablo, Nano Lett. **3,** 1405 (2003).
7. H.X. Zhou, G. Rivas, and A.P. Minton, Annu. Rev. Biophys. **37** 375 (2008).
8. R. Richert, Phys. Rev. B **54**, 15762 (1996).
9. G. B. McKenna, Eur. Phys. J. E **12**, 191 (2003).
10. C.J. Ellison and J.M. Torkelson, Nature Mater. **2**, 695 (2003).
11. F. Varnik, J. Baschnagel, and K. Binder, Phys. Rev. E **65**, 021507 (2002).
12. J. Baschnagel and F. Varnik, J. Phys: Cond. Matt. **17**, 851 (2005).
13. C. Bennemann, J. Baschangel, and W. Paul, Eur. Phys. J. B **10,** 323 (1999).
14. R.A. Riggleman, K. Yoshimoto, J.F. Douglas, and J.J. de Pablo, Phys. Rev. Lett. **97**, 045502 (2006).
15. P.P. Simon and H.J. Ploehn, J. Rheol. **44**, 169 (2000).
16. C.B. Roth, K.L. McNerny, W.F. Jager, and J.M. Torkelson, Macromolecules **40** 2568 (2007).
17. P. Scheidler, W. Kob, and K. Binder, J. Phys. Chem. B **108**, 6673 (2004).
18. E. Donth, *The Glass Transition: Relaxation Dynamics in Liquids and Disordered Materials* (Springer-Verlag 2000).
19. A. H. Marcus, J. Schofield, and S. A. Rice, Phys. Rev. E **60**, 5725 (1999).

20. E. R. Weeks and D. A. Weitz, Phys. Rev. Lett. **89**, 095704 (2002); F.P. Preparata and M.I. Shamos, *Computational Geometry* (Springer-Verlag, New York, 1985).
21. G. Adam and J. H. Gibbs, J. Chem. Phys. **43**, 139 (1965).
22. M. Vogel and S. C. Glotzer, Phys. Rev. Lett. **92**, 255901 (2004).
23. P.S. Sarangapani and Y. Zhu, Phys. Rev. E **77**, 061406 (2008); Phys. Rev. E **77**, 061406 (2008).
24. A. D. Dinsmore, et al, Applied Optics **40**, 4152 (2001).
25. See EPAPS Document No. xxxxx for additional data. For more information on EPAPS, see http://www.aip.org/pubservs/epaps.html
26. H. Hu and R. Larson, Langmuir **20,** 7436 (2004).
27. J. C. Crocker and D. G. Grier, J. Colloid Interf. Sci. **179**, 298 (1996).
28. V. N. Michailidou, G. Petekidis, J.W. Swan, and J. F. Brady, Phys. Rev. Lett. **102**, 068302 (2009).
29. N. Lacevic, F. W. Starr, T.B. Schrøeder, and S.C. Glotzer, J. Chem. Phys. **119**, 7372 (2003).
30. We determine the timescale at which ξ_4 is maximal by plotting ξ_4 vs. τ for varied volume fraction and thickness (see Supplemental Figure 5) which shows that ξ_4 is small on short timescales, peaks at intermediate timescales and decreases at long times .
31. P. Ballesta, A. Duri, and L. Cipelletti, Nat. Phys. **4, 550** (2008).
32. **L.** Berthier, G. Biroli, J.-P. Bouchaud, et al, Science **310**, 1797 (2005).
33. K.V. Edmond, C.R. Nugent, and E. R. Weeks (2010), arXiv: 1003.0856v1.

Figure Caption

FIG 1 (color online). Non-Gaussian parameter, α_2 measured in x-direction for ϕ = (a) 0.40 and (b) 0.43 at film thicknesses, H/d = 32 (squares), 24 (circles), 15 (triangles), and 11 (inverted triangles). The horizontal dashed lines indicate the regime where deviations from bulk behavior begin to occur.

FIG 2 (color online). a) Probability distribution, $P(\theta)$ of angles formed between the displacement vectors of nearest neighbors at the peak time in α_2 for ϕ = (a) 0.40, (b) 0.43, and (c) 0.46 at H/d = 52 (diamonds), 40 (stars), 32 (squares), 24 (circles), 15 (triangles), and 11 (inverted triangles). In all the cases, the string-like motion, indicated by the peak of $P(\theta)$ near 0, becomes prominent as the gap is reduced, which is schematically illustrated in panel (d) and (e) for ϕ = 0.40 and 0.43, both at H/d = 11, respectively, by cutting through a three-dimensional sample 3.5 μm thick at the peak-time in α_2. Arrows indicate the direction of motion for particles with the displacement, $\Delta r > 0.25$ μm and have the same length in all three directions, while "dots" indicate the motion in or out-of-plane.

FIG 3 (color online). Four-point correlation function for ϕ = 0.40 and H/d= (a) 23 and τ = 13 s (squares), 130 s (circles), and 1340 s (inverted triangles), (b) 15 and τ = 13 s (squares), 130 s (circles), 4784 s (triangles), 7150 s (inverted triangles), and 13560 s (left triangles), (c) 11 and τ = 13 s (squares), 130 s (circles), 1340 s (inverted triangles), 4784 s (triangles), 7150 s (diamonds), and 13560 s (left triangles); and ϕ = 0.43 and H/d = (d) 23 and τ = 13 s (squares), 2600 s (circles), and 7150 s (inverted triangles), (e) 15 and (f) 11 at the same times as the ones in panels (b)-(c). (g) The length scale, ξ_4, extracted from $g_4(r,\tau)$ close to the peak in the four

point correlation function using *Eq. 3* over the range of r=[2 μm, 9 μm] for ϕ = 0.40 (squares), 0.43 (circles), 0.46 (triangles), and 0.57 (inverted triangles) is normalized by the particle diameter, d, and plotted against H/d.

FIG. 4. Confinement length scales extracted from mean square displacement, non-Gaussian parameter as well as the four-point susceptibility at varied ϕ. Error bars indicate dispersion in thicknesses where the confinement effect begins in several independent experiments.

FIG 1.

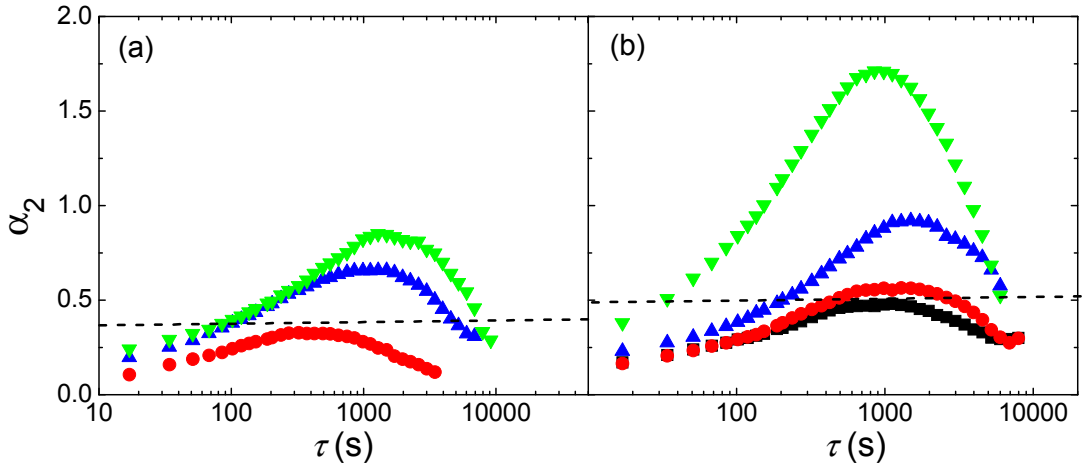
(a)
(b)
α_2
τ (s)
τ (s)
2.0
1.5
1.0
0.5
0.0
10
100
1000
10000
100
1000
10000

FIG 2.

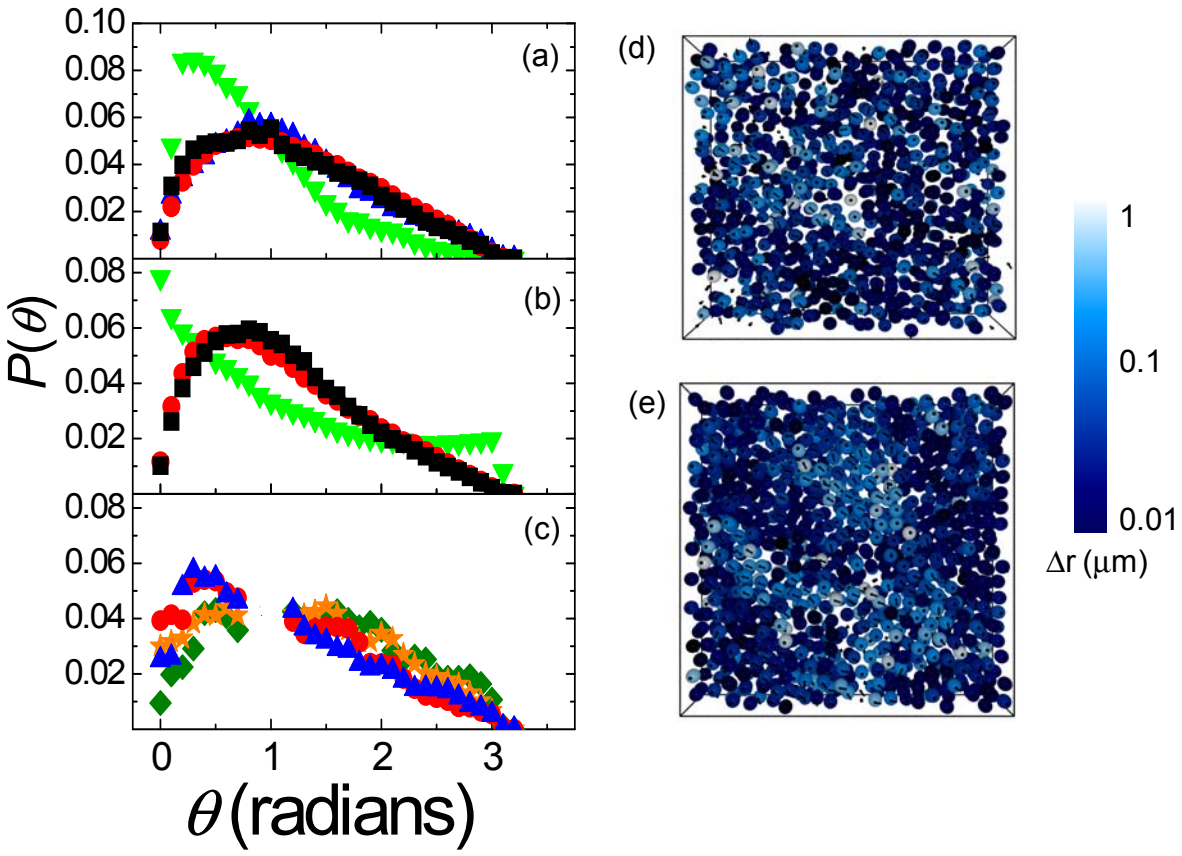

FIG 3.

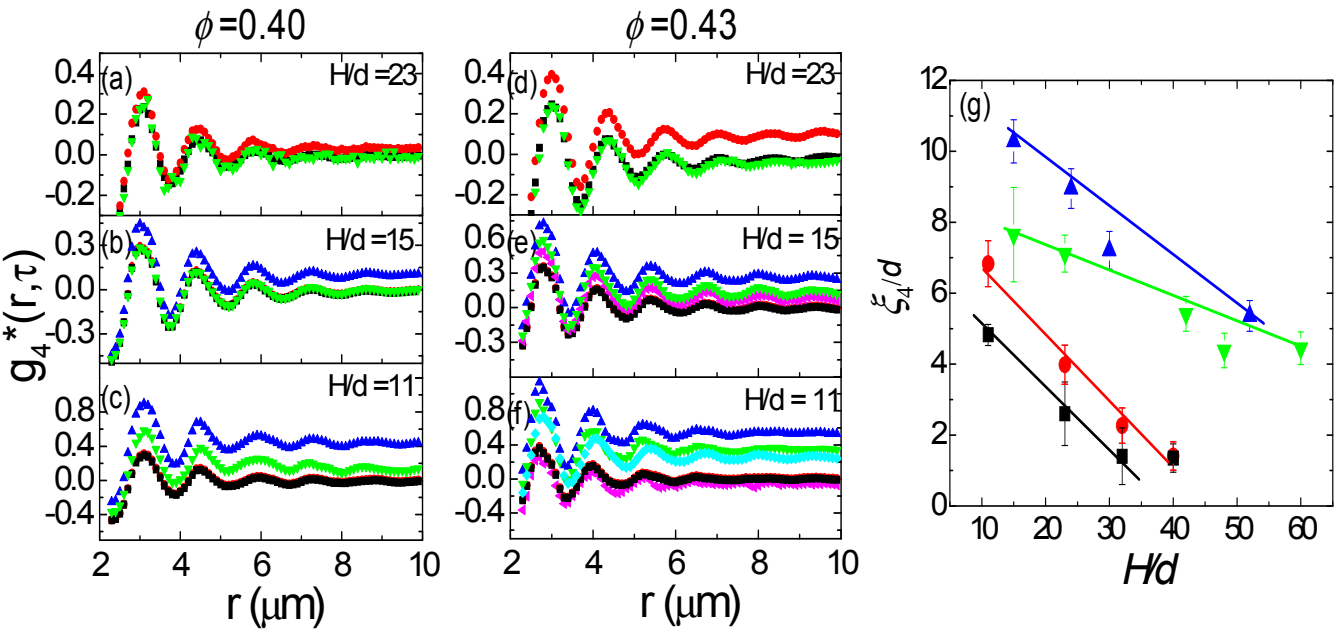
ϕ=0.40
ϕ=0.43
(a)
H/d =23
(b)
H/d =15
(c)
H/d =11
(d)
H/d =23
(e)
H/d = 15
(f)
H/d = 11
g4*(r,τ)
r (μm)
r (μm)
(g)
ξ4/d
H/d

FIG 4.